

RESEARCH ARTICLE

Wearable system for the measurement of gait cycle kinematic and kinetic signals

Manuela Gomez-Correa¹, Mariana Alegria¹, David Cruz-Ortiz² and Mariana Ballesteros^{1,2}

¹Centro de Innovación y Desarrollo Tecnológico en Cómputo, Instituto Politécnico Nacional, Mexico City, Mexico

²Medical Robotics and Biosignals Laboratory, Unidad Profesional Interdisciplinaria de Biotecnología, Instituto Politécnico

Nacional, Mexico City, Mexico

Corresponding author: Mariana Ballesteros; Email: mballesterose@ipn.mx

Received: 14 February 2025; Revised: 16 July 2025; Accepted: 22 September 2025

Keywords: design; sensors; embedded electronics; biomechanics

Abstract

Gait analysis is a fundamental tool in biomechanics and rehabilitation, as it evaluates human movements' kinematic and kinetic behavior. For this reason, high-precision devices have been developed. However, these require controlled environments, which generates a deficiency in the capacity of studies related to gait analysis in outdoor and indoor scenarios. Therefore, this article describes the development and testing of a wearable system to measure gait cycle kinematic and kinetic parameters. The methodology for the development of the system includes the assembly of modules with commercial surface electromyography (sEMG) sensors and inertial measurement sensors, as well as the use of instrumented insoles with force-resistive sensors, and the design of the software to acquire, process, visualize, and store the data. The system design considers portability, rechargeable battery power supply, wireless communication, acquisition speed suitable for kinematic and kinetic signals, and compact size. Also, it allows simultaneous assessment of sEMG activity, hip and knee joint angles, and plantar pressure distribution, using a wireless connection via Wi-Fi and user datagram protocol for data transmission with a synchronization accuracy of 576 μ s, data loss of 0.8%, and autonomy of 167 min of continuous operation, enabling uninterrupted data acquisition for gait analysis. To demonstrate its performance, the system was tested on 10 subjects without any neuromusculoskeletal pathology in indoor and outdoor environments, evaluating relevant parameters that facilitate a comprehensive analysis of gait in various contexts. The system offers a reliable, versatile, and affordable alternative for gait assessment in outdoor and indoor environments.

1. Introduction

Gait analysis is the systematic measurement and description of quantities that characterize human locomotion, representing a research area for medical and healthcare applications, such as the diagnosis and treatment of neurological or musculoskeletal diseases (Ziagkas et al., 2021), evaluation of orthoses and prosthetics (Chen et al., 2016), surgical procedures (Benson et al., 2018), and assessment of fall risks (Cimorelli et al., 2024). For these purposes, accurate measurements of gait parameters from kinematic (e.g., joint angle, angular velocity) and kinetic (e.g., plantar pressure, joint moment, surface electromyography [sEMG]) variables are necessary to evaluate musculoskeletal functions (Cimorelli et al., 2024).

© The Author(s), 2025. Published by Cambridge University Press. This is an Open Access article, distributed under the terms of the Creative Commons Attribution-NonCommercial licence (http://creativecommons.org/licenses/by-nc/4.0), which permits non-commercial re-use, distribution, and reproduction in any medium, provided the original article is properly cited. The written permission of Cambridge University Press must be obtained prior to any commercial use.



Reference techniques for kinematic and kinetic analyses require a professional motion capture system synchronized with force plates to provide reliable and accurate measurements of human motion, as well as skilled personnel to collect and analyze the data (Benson et al., 2018). Additionally, sEMG sensors are also incorporated to associate kinematic and kinetic variables with the subject's movement pattern and assess the musculoskeletal system (Negi et al., 2020).

The use of specialized equipment for gait analysis is demonstrated in several studies. For instance, Moreira et al. (2021) used the Trigno system with eight sEMG modules, the Oquis motion capture system with 12 cameras, and six Bertec force platforms to study 16 healthy participants walking at various speeds. Similarly, Bovi et al. (2011) collected kinematic, kinetic, and sEMG data from 40 healthy individuals using the SMART-E motion capture system, which consists of nine cameras, two Kistler force platforms, and eight ZeroWire sEMG modules. Another example is the work of Bagwell et al. (2024), which analyzed the biomechanics of 16 pregnant women and 16 matched controls using the Qualisys motion capture system, consisting of eight cameras, Bertec force platforms, and 16 Trigno modules. These systems require synchronization software to coordinate data acquisition, using either wired or wireless connections to send start and end signals. However, the high cost, extensive setup time, and advanced equipment needed limit these systems to specific clinical and research centers, preventing frequent or real-world gait analysis (Mobbs et al., 2022; Cimorelli et al., 2024).

For this reason, alternative gait analysis techniques have been developed using wearable sensors, which, thanks to their portability, allow the quantification of kinematic and kinetic patterns in natural environments and continuous monitoring. Such techniques involve attaching sensors (e.g., accelerometers, gyroscopes, magnetometers, force sensitive resistors [FSRs], flexible goniometers, and sEMG sensors) to various parts of the subject's body, such as the foot, thigh, and waist (Tao et al., 2012). Furthermore, the use of these sensors or systems enables the acquisition and recording of various spatiotemporal parameters, such as stride length, step duration, and stride speed, which are of great value in gait analysis. These parameters can be calculated using various algorithms for event detection and signal processing, such as calculating velocity using a direct and reverse integration approach and estimating stride displacement from the linear acceleration measured by the inertial measurement units (IMU) (Salis et al., 2023).

Using IMUs for kinematic variables and in-shoe pressure sensors for kinematic variables is commonly incorporated, as reported in several articles (Negi et al., 2021; Tsakanikas et al., 2023). Therefore, wearable sensors have been commercially developed, such as those manufactured by Xsens, InterSense, Technaid, IMeasureU, or Noraxon that offer a wide range of IMU-related products (Ribeiro and Santos, 2017), instrumented insole systems from Tekscan, Novel or Paromed GmbH (Ciniglio et al., 2021), or systems from Noraxon (Noraxon, n.d.) or Trigno (Delsys, n.d.). However, the simultaneous use of such systems still requires activation hardware; therefore, there is a need for systems development that allows synchronous quantitative kinematic, kinetic, and muscle activity assessment in outdoor environments and natural conditions.

Overall, the novelty of the system consists of having a low-cost, complete, replicable, and practical system for gait analysis applicable to different environments for the acquisition of kinetic and kinematic signals without the need for a controlled environment, such as a laboratory with high-cost equipment, which makes the system useful for various applications and analysis. The main contributions of this article are:

- A wearable system that comprises five wearable IMU-sEMG modules and a pair of instrumented insoles. The system's structural design is characterized by its ease of fabrication through 3D printing.
- Establish the synchronized data transmission protocol by implementing the User Datagram Protocol (UDP) as part of the wireless communication used in the IMU-sEMG modules and instrumented insoles.
- Software that allows structured storage of four sEMG signals, acceleration, angular velocity, and gravitational force signals from the five IMU-sEMG modules, along with the 48 plantar pressure signals in a CSV file, enabling further processing and evaluation of the signals.

• A Graphical User Interface (GUI) that allows the online visualization of four sEMG signals, the hip and knee joint angle signals, and 10 plantar pressure points per insole.

2. Preliminaries

Some elements used for gait analysis include vision systems (Fiker et al., 2020), sEMG modules (Agostini et al., 2020), inertial measurement units (Benson et al., 2022), force plates (Ichinohe et al., 2022), and instrumented insoles (Ziagkas et al., 2021). Depending on the device used, different parameters and measurement ranges are considered. This work includes sEMG sensors, IMUs, and insoles as part of the gait analysis system. From the earlier, the present section summarizes the parameters or ranges considered for developing the system.

In general, the sEMG signal has an amplitude that varies in the mV range, and its frequency is delimited between 0 and 500 Hz with a dominant energy region in the range of 50–150 Hz (Arteaga et al., 2020). Based on that and according to Nyquist's theorem, the minimum sampling rate of the system should be 1,000 Hz (Pancholi and Joshi, 2018; Rossi et al., 2021). It is important to remember that parameters such as frequency range or gain value may vary depending on the muscle group to be recorded. However, works like those presented in Daunoraviciene et al. (2021), Haque et al. (2022), Hussain and Park (2021), Moreira et al. (2021) have standardized acquisition frequencies from 1,000 to 2,000 Hz for the muscles involved in the gait and established equal acquisition gain for all recorded muscle groups.

IMU systems primarily collect spatial–temporal and kinetic information on human gait. Angular velocity and acceleration measurements are used in applications related to event detection or estimating the person's cadence (Wang et al., 2020), in the analysis of treatment and diagnosis of Parkinson's disease (Burtscher et al., 2024), and in the control strategies for exoskeletons in rehabilitation (Seo et al., 2019). Regarding the established parameters, it has been reported in the literature that the sampling frequency of the IMUs for gait analysis in different scenarios is above 100 Hz (Monoli et al., 2021; Yamamoto et al., 2022; Mason et al., 2023); likewise, the standard operating range established for the accelerometer in gait analysis applications is ± 8 or ± 16 g (± 78.48 and ± 156.96 m/s²) (Sarshar et al., 2021; Trautmann et al., 2021; Felius et al., 2022), between $\pm 1,000$ and $\pm 2,000$ deg/s for the gyroscope (Anwary et al., 2018; Caramia et al., 2018; Panebianco et al., 2018), and for the magnetometer, the value is usually around ± 12 G (Park and Yoon, 2021; Mobbs et al., 2022).

Also, wearable systems for measuring plantar pressure based on different sensing technologies, FSR, capacitive, or piezoelectric, are incorporated in insoles that are placed inside the footwear, allowing wireless transmission of data with low power consumption for the recording of mean and peak pressure values, displacement velocity of the center of pressure, and ground reaction forces (GRF). Those sensors must comply with a measurement range of at least 740 kPa with a spatial resolution of less than 10×100 mm, considering a sampling rate of 50 to 100 Hz (Wang et al., 2019).

3. Methods

3.1. System description

The main objective of the developed system is to have a portable and integral solution for gait analysis in outdoor and indoor environments. For this purpose, the wearable system integrates two main subsystems and the software, as Figure 1 illustrates. The first subsystem (see Figure 1a) consists of sEMG and IMU modules, and the second subsystem (see Figure 1b) corresponds to instrumented insoles for evaluating plantar pressure. Finally, Figure 1c represents the implemented software.

The software synchronizes the subsystems and controls the overall system, allowing the user to define acquisition times, visualize online signals, and qualitatively evaluate the subject during analysis. The following subsections provide details about each subsystem.

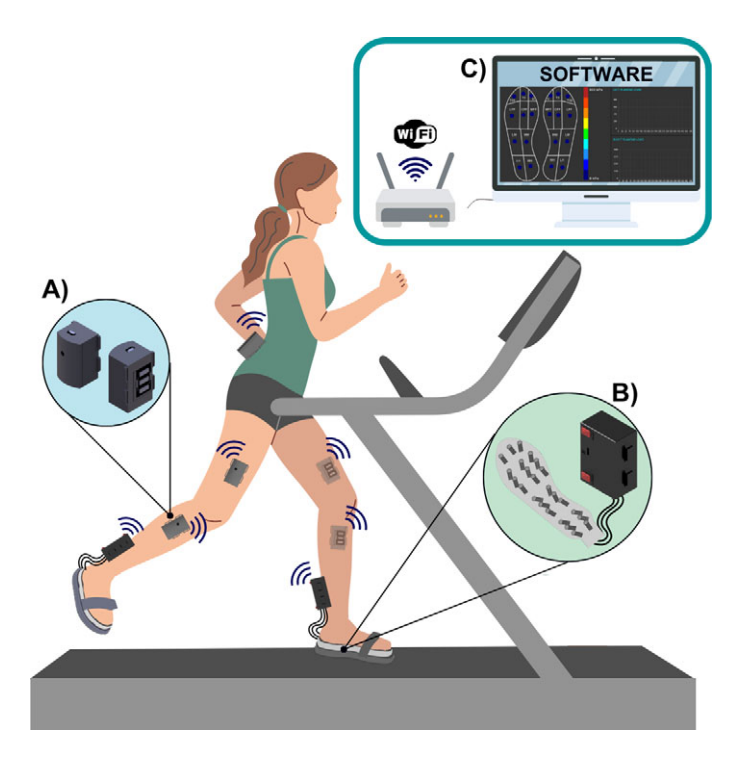


Figure 1. Subsystems integrating the gait cycle system. (a) IMU-sEMG modules. (b) Instrumented insole. (c) Software.

3.1.1. IMU-sEMG modules

The subsystem comprises five modules for acquiring information necessary for gait analysis, two for each lower limb and one for the torso. The inertial measurement used the LSM6DSOX and LIS3MDL 9-DoF Breakout Board, which is composed of a three-axis gyroscope, a three-axis magnetometer, and a three-axis accelerometer. The operating voltage is 3 or 5 V. On the other hand, for the muscular measurement, gravity analog EMG sensors were used, which measure sEMG with dry stainless steel electrodes and have an operating voltage range of 0 to 3 V. Additionally, this sensor features a filtering and amplification circuit, allowing for a biosignal with a baseline of 1.5 V.

The system utilizes a FireBeetle ESP-32 microcontroller to read and send information, as it incorporates Bluetooth and Wi-Fi modules into the board. Therefore, the UDP protocol was implemented to guarantee a sample rate higher than 1,000 Hz. In particular, the *Software description* section outlines the process for sending and processing the information. Finally, considering the system's operating voltage, the module contains a 3.7 V, 400 mAh Li-Po battery.

For the structural design, the requirements were to generate a compact design in terms of dimensions $(64 \times 36 \times 34 \text{ mm})$ to guarantee the correct positioning of the sensors implemented in the structure, specifically that the location of the electrodes generates an adequate contact for the acquisition of sEMG, and that the module can be easily positioned and adapted to the different anatomical dimensions of the subjects.

The module case was designed using Autodesk CAD Inventor 2021 software. Figure 2 shows each of the described elements of the module and their location in the developed structure, where the elements **A** denote the case, **B** correspond to the sEMG sensor, **C** to the IMU sensor, **D** to the microcontroller, and **E** to the Li-Po battery. The designed structural elements were manufactured using 3D printing with polylactic acid (PLA).

Additionally, as described in the *Preliminary* section, the sampling frequency for the sEMG sensor is 1,500 Hz. The IMUs parameters consider a sampling frequency of 100 Hz. Then, values of ± 16 g were

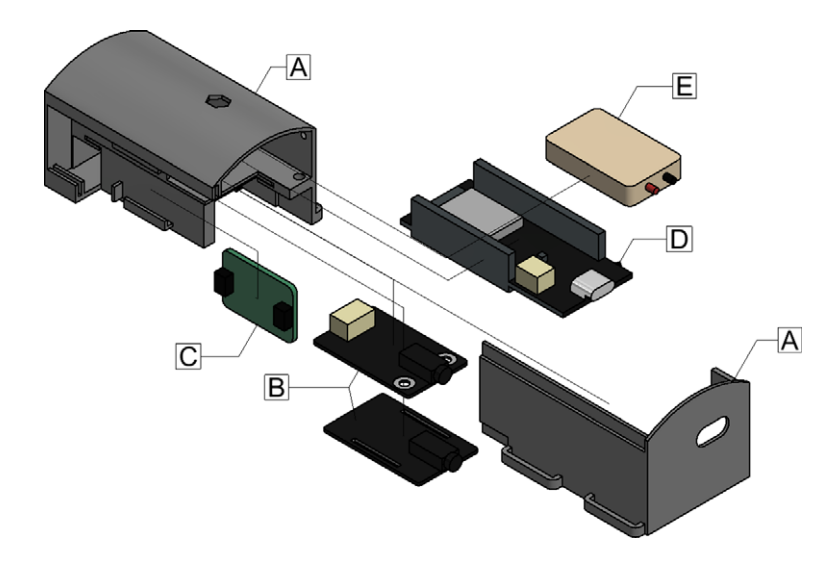


Figure 2. IMU-sEMG module assembly.

selected for the accelerometer; in the case of test subjects presenting unexpectedly large accelerations, this ensures the quality of the information. On the other hand, considering the bibliographic review, a value of $\pm 2,000$ deg/s (± 34.91 rad/s) was used for the gyroscope. Finally, a value of ± 12 G (± 0.0012 T) was defined for our system for the magnetometer.

Considering the earlier parameters, the preprocessing for sending the information in packets was defined. It is necessary to contemplate that the libraries used for the IMUs give the accelerometer (Ac) values in m/s², the gyroscope (Gy) in rad/s, and the magnetometer (M) in μ T. Additionally, a factor was multiplied by each value when sending the data, and an offset was added to all signals to avoid extra characters related to the decimal point and measurement sign. For the accelerometer, one decimal digit was contemplated, which means that if the value of each axis of the sensor varies in the range of ± 156.91 m/s² (i.e., ± 16 g), the value was multiplied by 10 and an offset of 2,000 was added. The earlier indicates that the sent value falls within the range of 431 to 3569. Then, for the gyroscope, two decimal digits were considered in the algorithm, and the operating range was ±34.91 rad/s (i.e., ±2,000 deg/s). Therefore, each value was multiplied by 100, and the offset was 5,000, generating a final value between 1,509 and 8,491. Finally, in the case of the magnetometer, the value was given by the sensor in μT (which means that the range of the value was in the range of ± 1200); for that the value did not contemplate a multiplied factor, but an offset of 2,000 was used. This resulted in a final range of values for the magnetometer between 800 and 3200. The offsets were selected slightly higher to ensure the values were not negative. In (3.1), C_i is denoted for the conversion of each measurement, where $i = \{Ac, Gv, M\}$ corresponds to the accelerometer, gyroscope, and magnetometer data, respectively.

$$C_{Ac} = Ac \times 10 + 2000,$$

 $C_{Gy} = Gy \times 100 + 5000,$
 $C_M = M + 2000.$ (3.1)

From the conversion, four characters corresponding to positive integers for each IMU measurement were necessary. Additionally, to represent the sEMG sensor, the sending process contemplated four digits, considering that the microcontroller used has a 12-bit analog-to-digital converter (ADC).

On the other hand, because the UDP protocol does not present confirmation messages during the sending and receiving of data, an extra character was added at the beginning of the string to identify the reception of a new data string in the software. From the earlier, two vectors were defined to send the information. The algorithm used interruptions to send the data at different frequencies, considering that for the IMUs, the sample rate was 100 Hz, and for the sEMG, 1,500 Hz. From this, (3.2) shows the architecture of the sent vector denoted by V_1 when the interruption indicates that both sensors need the sent information, then the vector V_2 in the Equation (3.3) exemplifies the sent vector for the interruptions that only contemplate the data of the sEMG.

$$V_1 = \{A, S, C_{Ac,x}, C_{Ac,y}, C_{Ac,z}, C_{Gy,x}, C_{Gy,y}, C_{Gy,z}, C_{M,x}, C_{M,y}, C_{M,z}\},$$
(3.2)

$$V_2 = \{A, S\},\tag{3.3}$$

where A defines the initial character, S represents the sEMG value, and the subindices x, y, and z define the measurement axis. Finally, the vector V_1 had a length of 41 characters, and 5 for V_2 .

3.1.2. Plantar pressure system

The subsystem consists of instrumented insoles to measure plantar pressure during gait. In particular, each insole consists of 24 FSR sensors and a data conditioning and transmission module, incorporated on a printed circuit board (PCB), utilizing the FireBeetle ESP-32 microcontroller to send the information via a Wi-Fi connection with a sampling rate of 50 Hz. Finally, the system requires two 3.7 V, 650 mAh Li-Po batteries.

The instrumented insoles incorporate FSR04 sensors from OHMITE with a working range of 7.71 to 1991.46 kPa and an active area of 5.6 mm, distributed in 10 anatomical sections of interest: hallux (H), second toe (T2), third to fifth toes (T35), medial forefoot (MFF), central forefoot (CFF), lateral forefoot (LFF), medial midfoot (MM), lateral midfoot (LM), medial heel (MH), and lateral heel (LH), as shown in Figure 3. The insoles were manufactured with a length of 25.5 cm. A thin antislip rubber film was applied to protect the active area of each sensor and ensure effective force transmission under distributed load conditions, as recommended by Tekscan (2024). For the data conditioning and transmission module, the

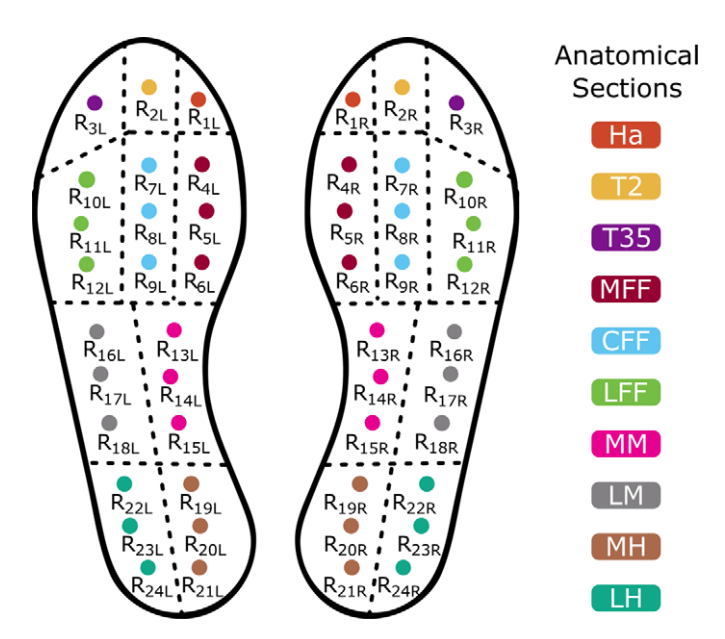


Figure 3. Sensors distribution into the anatomical sections of interest.

electronic instrumentation incorporates surface-mount devices (SMDs), all of which are in accordance with the specifications reported in Alegria et al. (2025).

For the structural elements, a compact design in terms of dimensions ($90 \times 65 \times 40$ mm) was considered, allowing the placement of the module on the back of the leg such that the module could be placed quickly and without interfering with the gait behavior.

The module shell was designed using Autodesk CAD Inventor 2021 software. Figure 4 shows each of the described elements of the module and their location in the developed structure, where the elements **A** denote the shell, **B** corresponds to the PCB, **C** to the implemented microcontroller, **D** to the Li-Po batteries, and **E** to the connection of the FSRs. The shell was fabricated using 3D printing with PLA.

As described in the preliminary section, the system has a pressure range of 150–800 kPa, considering a spatial resolution of 5.6 mm diameter with a sampling rate of 100 Hz. Each instrumented insole must be characterized to define the equation that describes the relationship between the pressure in each sensor according to the voltage generated in the data acquisition and transmission module, for which the methodology reported in Appendix A was followed.

The necessary preprocessing was defined for sending the information in a constant-length packet, considering the sending of the ADC value corresponding to each FSR with a resolution of 12 bits, sending four characters per sensor corresponding to positive integers. In addition, the protocol for sending the data is the same as that used in the IMU-sEMG subsystem. Therefore, an extra character must be added to identify the beginning of the information packet. From this, (3.4) shows the architecture of the sent vector information denoted by F_i .

$$F_{j} = \{A, C_{1,j}, C_{2,j}, C_{3,j}, \dots C_{23,j}, C_{24,j}\},$$
(3.4)

where j refers to the left insole (L) or the right insole (R), A defines the initial character, $C_{i,j}$ represents the value voltage registered in each resistive sensor $R_{i,j}$. Finally, the length of the vector was 97 characters.

3.1.3. Software description

For software development, the Node-RED tool, based on JavaScript, was utilized, specializing in creating applications for the Internet of Things (IoT). The software requirements included an easy-to-implement, intuitive, and functional design. To achieve this, the software consisted of three stages:

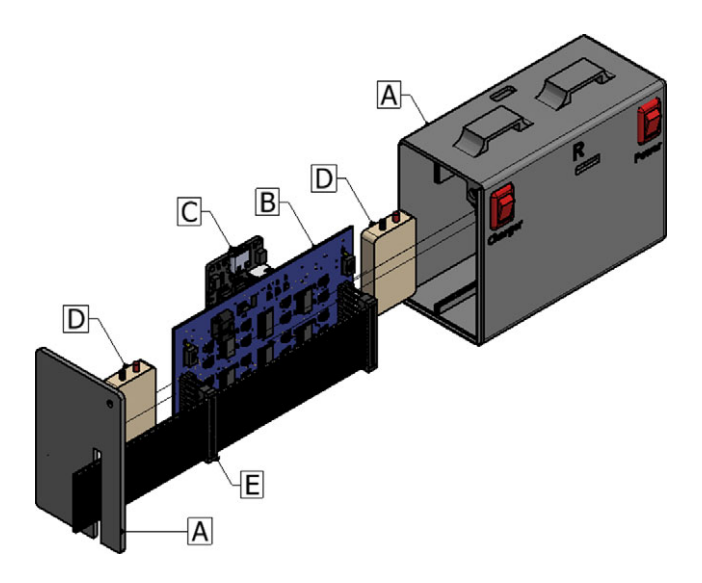


Figure 4. Instrumented insoles system. Ensemble of all the comprised elements.

3.1.3.1. Configuration stage. The user must enter the Wi-Fi network name of the device on which the software is running and its corresponding password; this information is saved in the GUI. Additionally, the user can choose the number of modules to be connected. Initially, the system considers the connection of the two instrumented insoles and five IMU-sEMG modules, whose locations are predefined and detailed in the following section (Experimental protocol). The user can connect up to four additional modules for complementary gait cycle analysis.

It is essential to note that the Wi-Fi network the user wishes to connect the system to does not require an Internet connection; therefore, a network can be created from a local or mobile device for operation. However, disconnecting the system from the network or losing connection during registration may cause data loss.

3.1.3.2. Connection stage. A new window displays each module or sensor configuration block based on the number of modules selected from the Configuration stage. Considering the network data that the user provided to the GUI (see Figure 5b) and the COM port selected (see Figure 5a), then the GUI creates a message with the information necessary for the device connection (see Figure 5c), and the software used the Serial protocol to send the message directly to the microcontroller, as seen in Figure 5d. The Serial message (Wc) corresponds to the network's name, password, and port used for the sensor's communication, as is shown in Equation (3.5).

$$Wc = Wssid + \ddot{A} + WPass + \ddot{y} + Uport$$
 (3.5)

where Wssid represents the service set identifier of the Wi-Fi network, Wpass represents the password, and Uport is the UDP port. The characters \ddot{A} and \ddot{y} are special characters for separating the sent information, which are recognized by the internal code of each FireBeetle ESP-32.

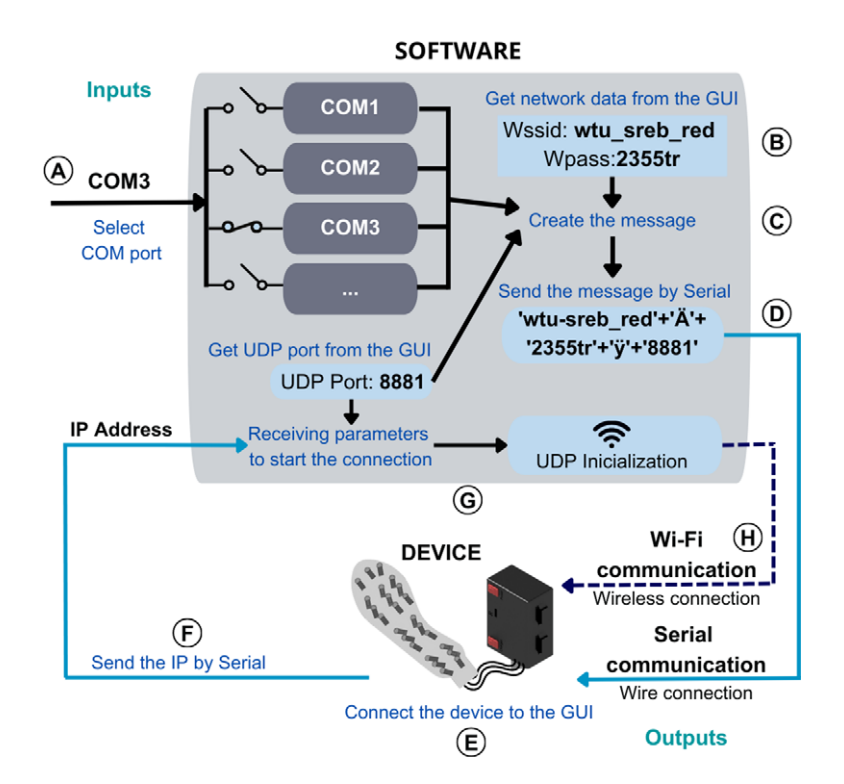


Figure 5. Wireless communication process of the subsystems and their interface software.

Once the microcontroller processes the information and connects to the Wi-Fi network (see Figure 5e), the ESP-32 sends the Internet Protocol (IP) address given to each device by the Serial protocol (see Figure 5f). Wireless communication can be initiated with the UDP and IP port established for each module or insole (see Figure 5g). Once the GUI receives the IP that confirms the connection, a green LED lights up in the connected module's block to indicate the correct connection of the devices to the network. Additionally, an RGB LED with a characteristic color is configured in the wireless devices in a way that allows the user to identify each sensor by its color quickly.

Finally, the wireless-connected devices initiate the Wi-Fi connection by clicking the save button, which sends a UDP message to all the connected ports. The ESP-32 identifies this message to initiate the continuous sending of the measurements considered in the system to analyze the gait (see Figure 5h). The diagram in Figure 5 describes the connection process using, as an example, one insole. It is important to note that the process detailed in Figure 5 must be followed for each of the system's devices, that is, the five IMU-sEMG modules and the two instrumented insoles.

The list below summarizes the steps considered in the connection stage.

- 1. Connect the device to a COM port
- 2. Select in the GUI the COM port where the device is connected
- 3. Get the network information from the GUI
- 4. Get from the GUI the UDP port set for the device
- 5. Create a message with connection information
- 6. Send the message via Serial communication
- 7. Make the connection of the device to the network with the message received
- 8. Send by Serial communication the IP given to the device after connection
- 9. Save the IP and UDP port of each device in the GUI
- 10. Initialize the UDP communication
- 11. Send the sensor information by UDP

Remark 3.1. The GUI assigns a specific port to the device; then, the information is received through different channels. In that sense, the only way that the information for the sensor has a relevant loss of information (up to 3%) is because the sensor needs to be charged, the speed of the network decreases, or the circuit is damaged.

3.1.3.3. Acquisition stage. This stage of the software is divided into four main blocks: storage, visualization of plantar pressure data, visualization of the inertial measurements data, and visualization of the sEMG data (see Figure 6).

The storage block (see Figure 6a) saves the information. It has two text boxes: one for the file name and the second to indicate the computer's address where to save the information. Additionally, it has an LED, as well as start and end buttons. These buttons allow the user to set when to start storing the data and when to end it; the LED turns green during storage or red in other cases.

The second block (see Figure 6b) corresponds to the visualization of the plantar pressure data. It comprises a silhouette of two insoles divided into the 10 relevant anatomical sections of the foot presented in Figure 3; in this section, the mean pressure of each region is calculated according to Equation (3.6)), to display the pressure value of the 10 points on a color scale according to the measurement color bar observed in the GUI. In this way, the user is able to do an online qualitative assessment of the pressure distribution during gait. In addition, two graphs are included showing the total plantar pressure exerted on each foot, defined by Equation (3.7).

$$PA_{k,j} = \frac{1}{n} \sum_{i=1}^{n} P_{i,j},\tag{3.6}$$

Figure 6. Graphical user interface.

where $PA_{k,j}$ is the pressure generated in the footprint at the kth region in kPa, $k = \{1, 2, ..., 10\}$, $i = \{1, 2, ..., 24\}$, j defines the side $(j = \{L, R\})$, n refers to the number of sensors located into the region, and $P_{i,j}$ is the pressure measured by the i,jth resistive sensor, also in kPa.

$$PP_j = \frac{1}{24} \sum_{i=1}^{24} P_{i,j} \tag{3.7}$$

where PP_j is the pressure generated in the footprint by the contact with the ground in kPa, $i = \{1, 2, ..., 24\}$, j define the side $(j = \{L, R\})$, and $P_{i,j}$ is the pressure measured by the i,jth resistive sensor, also in kPa.

The IMU display block (see Figure 6c) shows an approximation of the inclination angle of the hip and knee, which is calculated using the accelerations given by the IMU sensor (Takeda et al., 2009). Equation (3.8) describes the equation used to estimate the angles concerning the gravitational acceleration vector. Additionally, a low-pass filter and an average function were applied at the interface to reduce the signal noise.

$$\alpha_{i,j} = \cos^{-1}\left(\frac{Ac_i}{\sqrt{Ac_x^2 + Ac_y^2 + Ac_z^2}}\right),$$
(3.8)

where $a_{i,j}$ represents the angle, *i* defines the axis $(i = \{x, y, z\})$, and *j* the joint $(j = \{hip, knee\})$.

It is essential to note that the calculation of angles performed in the GUI is an approximation of the actual angles. Possible errors must be considered because the calculation only uses the accelerometer, and its frequency response might introduce errors. Considering that the IMU sensors are sensitive to noise, the information from the accelerometers, gyroscopes, and magnetometers is stored from the GUI in a way that the user can postprocess the information and apply more accurate estimation algorithms, such as those based on optimization methods or quaternions (Madgwick et al., 2011; Choi et al., 2021; Rahman et al., 2023). Finally, for the sEMG visualization (see Figure 6d), the last 1,000 values collected by the sensor were taken and processed for visualization in Volts. Additionally, Gauge-type graphs were added to depict the energy of the data window displayed.

3.2. System validation

The validation of the system developed for the measurement of kinematic and kinetic parameters/signals during the gait cycle considers the evaluation of the synchronization of signal acquisition, data loss in

wireless transmission, and system autonomy in order to determine the robustness of the system, considering fundamental aspects for its implementation in the analysis of gait in outdoor environments and to guarantee an accurate interpretation of the data. The main results of the following validation methodologies are discussed in Section 4.

3.2.1. Data synchronization

The proper synchronization of the modules that make up the system was evaluated by comparing the time stamps generated in each acquisition, for which each module generates a square wave at the beginning of the wireless transmission, where the high pulse corresponds to the processing and sending of the data packet. The resulting square wave outputs were recorded using a digital oscilloscope (Tektronix TBS1102B-EDU) and processed through a custom Matlab script to calculate the synchronization accuracy.

3.2.2. Data loss

Considering that the system uses Wi-Fi connection and the UDP communication protocol for real-time wireless data transmission, data loss was evaluated under different connectivity conditions. Tests are carried out using public and private networks to quantify the percentage of packets not received in the GUI with respect to the total packets sent by the modules that integrate the system, knowing that for each second recorded, 1,500 samples of each sEMG signal must be obtained, while for IMUs and instrumented insoles, a total of 100 samples per module must be recorded.

3.2.3. System autonomy

Energy consumption tests were performed under continuous operation conditions to determine the system's autonomy. The battery life of the IMU-sEMG modules was measured while transmitting continuous data until fully discharged. To evaluate the autonomy of the instrumented insoles, a static test of constant use was performed by placing a known mass on the insole to record the pressure every 60 min and removing it after 300 min to evaluate the long-term stability of the insole. The results were compared with the technical requirements of the system and with reference values of other similar devices used in gait analysis.

3.3. Experimental protocol

3.3.1. Participants

Ten healthy participants $(20 \pm 5 \text{ years}, 70 \pm 15 \text{ kg}, 165 \pm 15 \text{ cm}, five males, five females)}$ were recruited. The purpose of the study was explained to them, and they were asked to sign the informed consent form. The study protocol was reviewed and approved by the Secretary of Research and Postgraduate Studies of the IPN (SIP-20250223 and SIP-20250253), which is responsible for approving research protocols following the ethical standards defined in the Declaration of Helsinki. The tests were performed at the Medical Robotics and Biosignals Laboratory, UPIBI-IPN.

Inclusion criteria included healthy participants without any neuromusculoskeletal, cardiovascular, pulmonary, or neurological disease and with a foot length between 24 and 26 cm. For each subject, age, gender, weight, height, occupation, and the anthropometric measurements of the lower limb (leg length, knee width, ankle width, foot width, foot length, and heel width) were collected.

3.3.2. System setup

The system considers five IMU-sEMG modules attached to specific locations and the two instrumented insoles, as shown in Figure 1. Although it is possible to add more modules, we used five for this protocol. If additional modules are required, their placement will depend on the type of analysis.

The use of the IMUs of the modules aims to approximate the angular range of motion of the torso, hips, and knees. For this reason, the lumbar area at the level of the iliac crest was considered for the module's

location, which is responsible for torso tilt. On the other hand, in the modules located in the upper leg, the vastus lateralis muscle of each leg was considered. For the location of this sensor, the electrodes were placed at 2/3 of the line from the anterior superior iliac spine to the lateral side of the patella. Additionally, for the lower leg, the peroneus longus muscle was considered a strategic point for the modules' location, with approximately three quarters of it placed on the line between the tip of the lateral malleolus and the tip of the head of the fibula. The location of all the electrodes was considered according to the recommendations of the SENIAM project (Hermens et al., 2000).

On the other hand, to calculate the joint angles, the modules were placed vertically as close as possible to the sagittal plane, considering the locations described earlier. The instrumented insoles were placed in the participants' shoes, and the module was attached to the back of the lower leg without interfering with the placement of the IMU-sEMG modules.

3.3.3. Experiment design

Three experiments were defined: evaluation, indoor, and outdoor experiments. Based on this, the tests to be performed by the subjects were defined as described below. Also, Figure 7 summarizes the steps involved in each test.

3.3.3.1. Evaluation. The evaluation test was performed to check the correct functioning of the device and its measurements, specifically for the IMU-sEMG modules. To validate the proper calculation of the torso, hip, and knee ranges of motion, the user stands with his legs straight and tilts his torso to its maximum capacity for three repetitions; then, he is asked to sit down and stand up three times from a chair. In the case of the insole, as it has a specific characterization process, its correct functioning is evaluated during another stage.

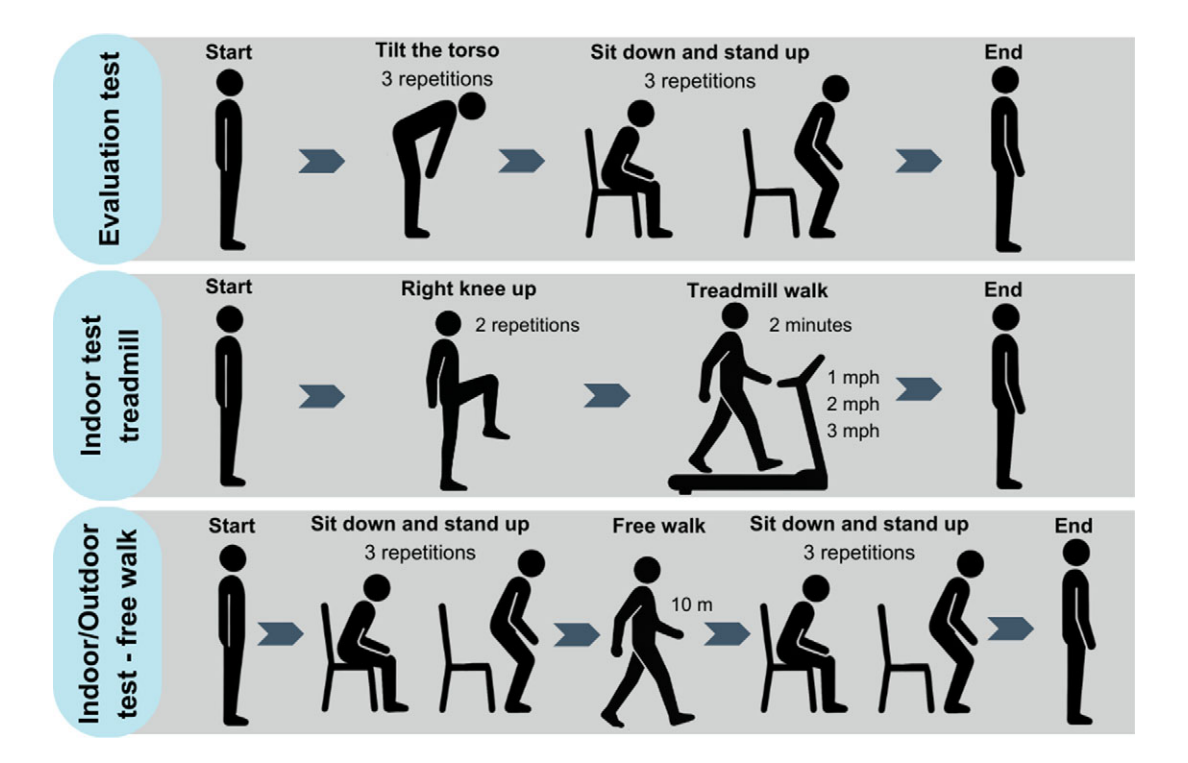


Figure 7. Test design.

3.3.3.2. Indoor. The indoor protocol involved two tests: one to measure the system's performance at different speeds and the second to compare the system's performance between the indoor and outdoor experiments.

The speed test was conducted on a treadmill at three controlled velocities (2, 2, and 3 mph), recording 1-min trials. First, once the system was placed on the subject, the operation of the devices was checked using the software. Next, the participant is familiarized with the use of the treadmill. The test begins by driving the right knee up, standing for 2 s twice, and then starting the treadmill walk at the different velocities, allowing for a 2-min rest between tests. These tests are performed three times. Also, a digital pedometer assessed the speed, time, and number of steps each subject took over the set meters.

For the second test, the user starts by sitting and standing three times on a chair, then walks 10 m in a straight line at a self-controlled speed, and finishes by performing three more actions of standing and sitting on a chair. This experiment was repeated three times, with a rest time of 2 min between each trial. This same process was conducted in the Outdoor experiment.

3.3.3.3. Outdoor. The outdoor protocol involved the subject walking on grass continuously in a straight line for 10 m. A digital pedometer assessed the speed, time, and number of steps each subject took over the set meters. First, once the subject used the systems, the devices were checked for functionality using the software. The participant then performed the test in the open field. The test begins with the subject sitting down and getting up from a chair three times, then walking in a straight line for 10 m at a self-controlled speed, ending with the subject sitting down and getting up from a chair three more times, allowing a 2-min break between trials. Blue lines marked the start and end points of the walking area. Three trials per subject were obtained in this phase.

4. Results and discussion

Figure 8 illustrates the operation of the designed system in outdoor and indoor environments. In particular, Figure 8a shows the IMU-sEMG modules, which were adjusted to the body with elastic belts to ensure the correct contact of the electrodes with the skin, adapting to different body types. These were placed as close as possible to the sagittal plane to reduce errors in the calculated angles due to the rotation of the IMUs. On the other hand, Figure 8b shows one of the instrumented insoles. It is evident how the insoles fit the test subject's regular footwear, showcasing the system's adaptability to different shoe types. The module at the back of the lower leg ensures no interference or discomfort during the gait cycle. Subsequently, Figure 8c shows how the software performs, adapting to different user preferences and providing visual feedback on the person's gait, as well as the calculation of the angles, the average plantar pressure, and the online visualization of sEMG signals.

Subsequently, the operation of the system developed was validated. For this purpose, the results of eight tests were recorded to evaluate the synchronization of the system, obtaining an average

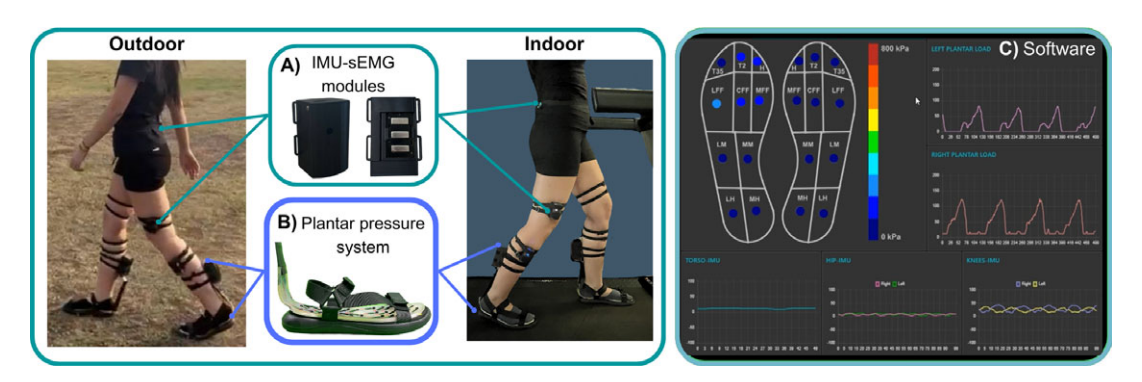


Figure 8. Wearable system for gait cycle. (a) IMU-sEMG modules. (b) Instrumented insole. (c) Software.

synchronization accuracy of $576 \pm 8 \,\mu s$ between the activation of the first and last module connected to the GUI. That means a latency of $96 \,\mu s$ between two subsequent sensors. Then the system's synchronization, specifically for each module, would depend on the sampling frequency and the nature of the recording signal. These results suggest that the system is capable of acquiring and synchronizing signals with adequate accuracy for application in gait cycle analysis.

On the other hand, the data loss was evaluated considering the signals collected in the tests of the different subjects. With the start and end time for each test stored in the generated CSV files and considering the sampling frequency of each module, the number of samples each signal should have was computed. From this analysis, it was observed that when the system is connected to a public network, there can be a data loss of up to 2.18%, while if a network is used only for the system's operation, a maximum data loss of 0.8% was reached. The earlier verifies the communication protocol's correct functioning and data reception at the interface.

Regarding system autonomy, the battery life of the sEMG-IMU modules was evaluated during continuous data transmission. A 3.7 V, 400 mAh Li-Po battery was used in each module, which allowed uninterrupted wireless transmission for 167 min before being completely depleted. This operating time indicates that the system is capable of continuous operation during prolonged analysis sessions without interruption, making it viable for research applications. As a result of the static test of the stability evaluation of the instrumented insole, Table 1 reports the percentage of variation of 11 activated sensors $(R_{i,j}, i = \{1, 2, ..., 24\}$ denotes the number of sensor, j = L, R denotes the laterality) when placing a known mass of 14 kg on the insole, where it can be concluded that in continuous use, the maximum variation is 9.25%, which evidences the long-term stability for studies of walking cycle for five continuous hours, as recommended by Giacomozzi et al. (2012) for plantar pressure measurement systems. Once the system's operation was verified, the analysis of the signals for the evaluation tests was performed.

The validation test performed a general study of the acquired signals. Specifically for the sEMG signals and the angles calculated with the signals obtained for the IMUs, it was observed that the information was synchronized, and the visual characteristics of the signal were congruent in the different test segments. Figure 9 shows the hip angle, knee angle, vastus lateralis sEMG signal, and peroneus longus sEMG signal throughout the evaluation test.

From Figure 9, it was observed that during the execution of the standing and sitting actions, a higher effort and activation of motor fibers of the sEMG signals were registered, evidenced by a higher density and magnitude of the graph during these segments. On the other hand, at the high points of the signals (i.e., at times of 7, 10, and 14 s), the sEMG signals present a low amplitude, which corresponds to the segments of the test where the participants were sitting on the chair, and there was no muscle activation. As for the hip angles, it was observed that when the participants were standing upright, the angles for both the knee and the hip were approximately 0, but for the 7, 10, and 14 s in which the action of standing and sitting was performed, maximum values of approximately 79° for the hip and 88° for the knee were achieved. The earlier evidence demonstrates the congruence between the data collected and the various actions performed during the test.

Considering that the calculation of both the knee and the hip was simplified on the sagittal plane from Equation (3.8), the angle obtained for both the knee and the hip was analyzed with all the test subjects. In the postprocessing of this signal, a low-pass digital filter with a cut-off frequency of 10 and a smooth

| | Sensor (%) | | | | | | | | | | |
|------------|------------|----------|----------|----------|-----------|------------------|------------------|------------------|------------------|------------------|------------------|
| Time (min) | R_{1R} | R_{2R} | R_{3R} | R_{4R} | R_{10R} | R _{11R} | R _{17R} | R _{20R} | R _{22R} | R _{23R} | R _{24R} |
| 60 | 1.01 | 1.54 | 0.76 | 1.30 | 0.47 | 3.09 | 3.61 | 2.48 | 0.45 | 1.00 | 2.09 |
| 120 | 0.28 | 0.95 | 0.26 | 1.49 | 1.18 | 2.88 | 4.73 | 6.77 | 0.82 | 0.37 | 0.16 |
| 180 | 0.27 | 0.42 | 0.33 | 1.06 | 0.67 | 5.98 | 3.19 | 8.68 | 0.52 | 0.32 | 0.01 |
| 240 | 0.68 | 0.94 | 0.05 | 0.25 | 0.15 | 4.70 | 6.51 | 6.02 | 0.01 | 0.12 | 0.25 |
| 300 | 0.54 | 1.49 | 0.65 | 0.18 | 0.60 | 1.41 | 4.79 | 9.25 | 0.71 | 0.20 | 0.02 |

Table 1. Variation of pressure in continuous use

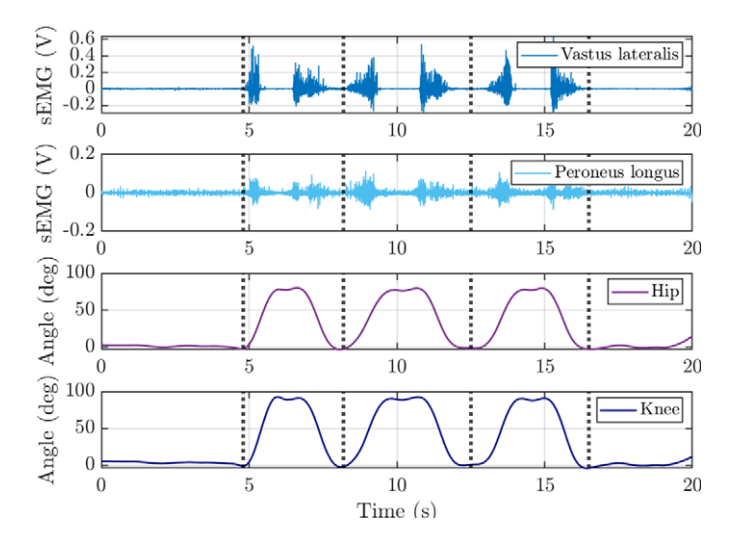


Figure 9. Evaluation test signals.

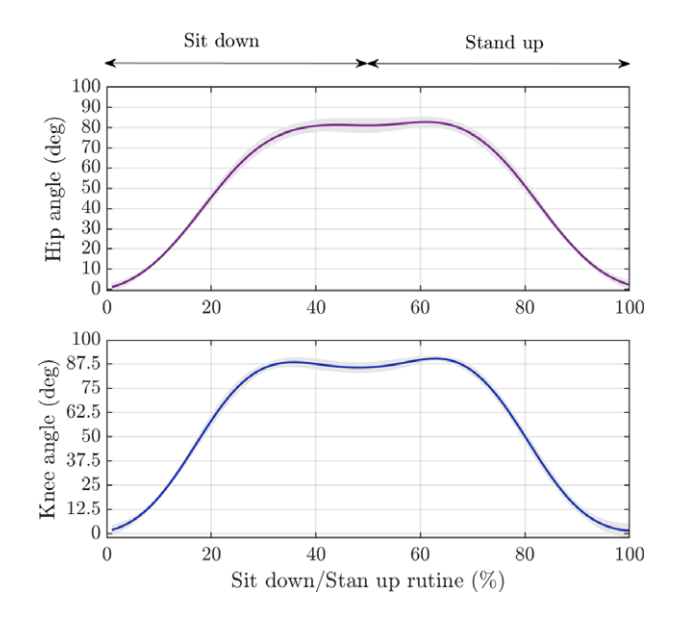


Figure 10. Evaluation test – joint angles.

function was applied to the signal. Then, the signals were segmented, obtaining all the data corresponding to sitting and standing up from the chair. From this, the standard deviation of the data collected was calculated to demonstrate the calculation's stability in a controlled and repetitive movement. Figure 10 shows the average graph of the hip and knee angles obtained during the evaluation test and their respective standard deviation, corresponding to approximately 2.3022° for the hip angle and 2.2901° for the knee.

Once the evaluation test showed the correct system functioning, the indoor tests were performed considering the different speeds. Figure 11 shows the hip and knee angles and the EMG signals of the vastus lateralis and peroneus longus obtained for one of the subjects during the three speeds. The graph demonstrates that both the hip and knee angles are minimal for the lowest speed. Likewise, the amplitude of the vastus lateralis sEMG signal is low compared to the other speeds. Thus, as the speed increased, sEMG signals with higher amplitude and density, and knee and hip angles with a more extensive range of

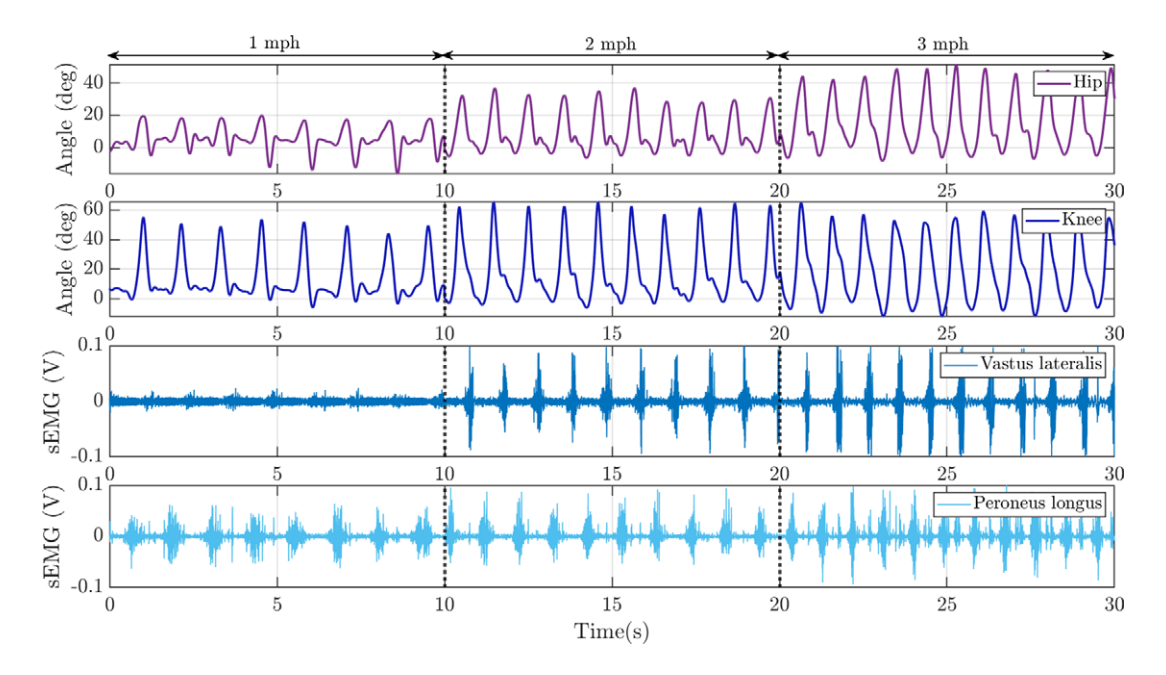


Figure 11. Indoor test – system performance.

motion were observed. The earlier is a congruent result since increasing the walking speed of the test subjects requires greater physical effort, which translates into sEMG signals with greater activity and the generation of a greater stride length to achieve the established speed.

On the other hand, a quantitative analysis of the sEMG signals was performed from the calculation of parameters such as the power to observe the amount of work per second in the signal, the signal-to-noise ratio as an index of the existing proportion between the power of the signal that is transmitted and the power of the noise registered during the acquisition; for the slope to sign change that represents the number of times that the slope of the EMG signal changes signs and the waveform length feature evaluate the complexity of the signal. Considering the earlier, Table 2 shows the average of the characteristics during the three trials for the vastus lateralis, and Table 3 shows the results for the peroneus longus muscle.

Tables 2 and 3 show that the calculated characteristics do not present a very high deviation between the trials, demonstrating the system's stability by obtaining similar values during different tests over time. Likewise, it was observed that the value for the signal-to-noise ratio parameter remained approximately constant during all the tests, which proves the correct functioning of the implemented filters and the

| Velocity (mph) | Feature | Trial 1 | Trial 2 | Trial 3 |
|----------------|----------------------------|---------|---------|---------|
| 1 | Power | 1.8885 | 1.8887 | 1.8885 |
| | Signal-to-noise ratio (dB) | 36.54 | 36.54 | 36.54 |
| | Slope sign change | 65 | 83 | 73 |
| | Waveform length | 48.5190 | 49.7308 | 40.5218 |
| 2 | Power | 1.8884 | 1.9025 | 1.8865 |
| | Signal-to-noise ratio (dB) | 36.54 | 36.62 | 36.53 |
| | Slope sign change | 171 | 281 | 153 |
| | Waveform length | 60.1093 | 55.0546 | 43.8935 |
| 3 | Power | 1.8897 | 1.8894 | 1.8877 |
| | Signal-to-noise ratio (dB) | 36.55 | 36.55 | 36.54 |
| | Slope sign change | 223 | 271 | 224 |
| | Waveform length | 64.3301 | 55.2155 | 46.8935 |

Table 2. Vastus lateralis sEMG features

| Velocity (mph) | Feature | Trial 1 | Trial 2 | Trial 3 |
|----------------|----------------------------|---------|---------|---------|
| 1 | Power | 1.9453 | 1.9450 | 1.9448 |
| | Signal-to-noise ratio (dB) | 51.13 | 51.13 | 51.12 |
| | Slope sign change | 48 | 91 | 73 |
| | Waveform length | 33.5699 | 36.7254 | 33.3922 |
| 2 | Power | 1.9437 | 1.9452 | 1.9445 |
| | Signal-to-noise ratio (dB) | 51.12 | 51.13 | 51.12 |
| | Slope sign change | 129 | 149 | 153 |
| | Waveform length | 36.5926 | 39.3517 | 38.7633 |
| 3 | Power | 1.8898 | 1.9442 | 1.9446 |
| | Signal-to-noise ratio (dB) | 51.12 | 51.12 | 51.12 |
| | Slope sign change | 280 | 231 | 224 |
| | Waveform length | 54.6614 | 48.6998 | 50.0018 |

Table 3. Peroneus longus sEMG features

correct placement of the electrodes on the skin in order to reduce the noise caused by the incorrect contact of the electrodes or the movement of the subject.

Additionally, it was observed that for the waveform length feature, the value of this parameter increased when the test speed increased. The earlier is congruent since a higher speed generates higher electrical activity, thus creating a more complex and robust signal in density and magnitude. Then, it was observed that the slope sign change parameter was also directly proportional to the speed of the test, indicating that the change of the slope of the signal increases as a consequence of a major collection of motor fibers or a higher effort, which generates a signal with a significant number of variations. Finally, the signal-to-noise ratio feature showed a higher value for the peroneus longus compared with the vastus lateralis. This can be a consequence of a better placement of the sensor, a high electrical activity of this muscle group during human gait, or the presence of less body fat over this region.

Then we proceeded to the analysis of the test that contemplated standing and sitting, and a free walk of 10 m, performed for indoor and outdoor environments. Figure 12 shows the signals of one of the subjects for the planted scenarios, showing signals with very similar visual characteristics, such as the execution

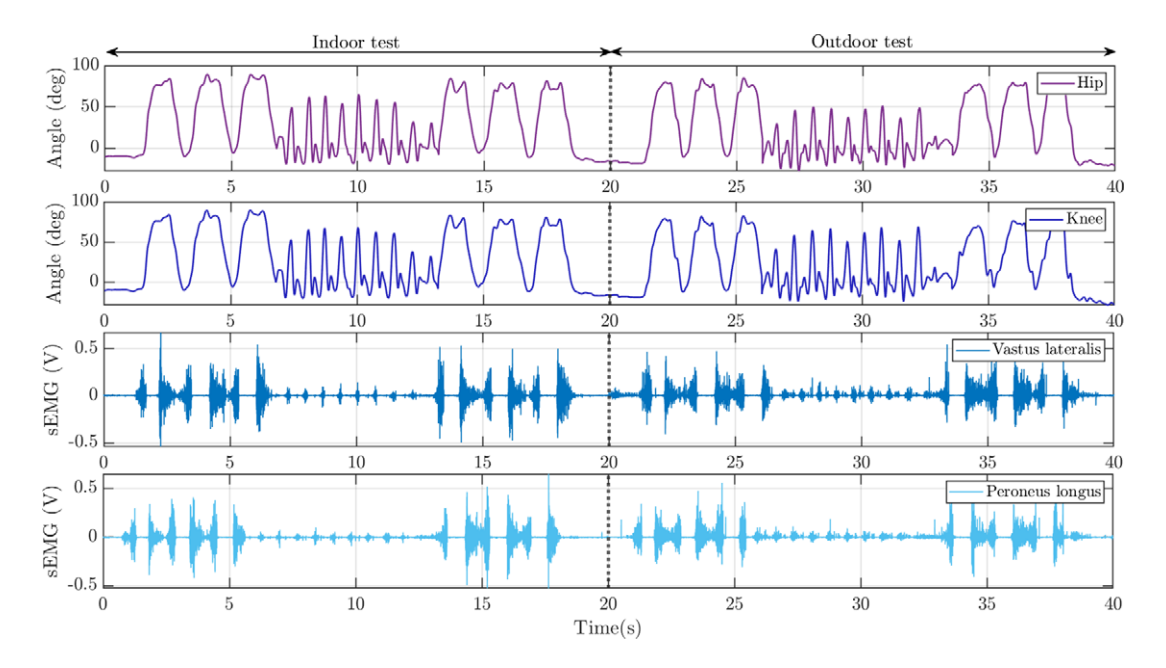


Figure 12. Indoor versus outdoor test performance.

| Muscle | Feature | Indoor test | Outdoor test | |
|------------------|----------------------------|-------------|--------------|--|
| Vastus lateralis | Power | 0.0033 | 0.0019 | |
| | Signal-to-noise ratio (dB) | 41.07 | 38.24 | |
| | Slope sign change | 108 | 117 | |
| | Waveform length | 76.6724 | 65.9330 | |
| Peroneus longus | Power | 0.0024 | 0.0019 | |
| <u> </u> | Signal-to-noise ratio (dB) | 32.8614 | 30.5983 | |
| | Slope sign change | 45 | 74 | |
| | Waveform length | 67.2055 | 60.9381 | |

Table 4. Indoor versus outdoor test - sEMG features

time of the exercises and amplitude. Only a slight attenuation of the sEMG signals is observed in the case of the outdoor test compared to the indoor test; likewise, the range of motion of both the hip and the knee during the free walk also presents a lower range than that recorded for the indoor test. This behavior occurred in 82.4% of the signals recorded for all subjects during the three trials. On the other hand, to demonstrate a quantitative comparison of the results obtained for the sEMG signals, the same parameters were calculated in Tables 2 and 3. The results are presented in Table 4 for both the indoor and outdoor environment tests.

From Table 4, it was observed that the signal power was lower in the case of the outdoor test; in addition, the signal-to-noise ratio was higher in the outdoor test; this analysis suggests that a possible cause is that walking on a floor that is not uniform can generate the contribution of other muscle groups generating an attenuation of the magnitude of the signals acquired in the outdoor test, in addition the non-uniformity of the floor can cause extra movements on the modules which could generate an acquisition of additional noise on the baseline. The earlier proposes a more extensive analysis of the hypothesis raised for future work. In addition, due to the simplified calculation used for the hip and knee angles computation and considering the IMU's high susceptibility to noise caused by motion, it is suggested as future work to implement an optimization algorithm for the joint angles. However, the system collects the nine signals from each IMU (three from the gyroscope, three from the magnetometer, and three from the accelerometer) for the implementation of a more robust algorithm in postprocessing.

Furthermore, to extract relevant features from the plantar pressure signals, the recorded values were averaged across trials for the dominant limb. Figure 13 presents the results obtained from the indoor (1, 2, and 3 mph) and outdoor (free gait) tests performed by a healthy female participant.

Finally, for the insoles analysis and to synthesize the data collected, Table 5 shows the peak force values (FA) during maximum weight acceptance, the time required to reach this phase (TA), the peak force in the mid-stance phase (FB) and its corresponding time (TB), the peak force in push-off (FC) together with the time to reach it (TC), the time to the end of the stance phase (TD), and the duration of the swing phase (TS) obtained in each experiment. It is noted that the increase in gait velocity is directly related to an increase in peak force values, especially peak FC, as reported in Yu et al. (2021). Moreover, in all conditions, peak FC presents the highest pressure values, followed by peak FA and finally by peak FB, which is consistent with gait biomechanics. The reduction in TA, TB, and TC times is observed with increasing speed, suggesting a more dynamic and efficient gait pattern, characterized by a faster transition between the different support phases of the gait cycle; similarly, TD and TS times are observed to remain relatively constant at all speeds, indicating that the gait pattern remains stable regardless of speed.

5. Limitations

FSR technology limitations: Due to the inherent characteristics of FSR technology, factors such as
sensor placement sensitivity, potential adhesion issues, and calibration drift over time can affect the
accuracy of absolute pressure measurements. In this study, the system was primarily designed for the
synchronous acquisition of kinematic and kinetic data. Although the current sensor configuration
does not achieve the resolution of laboratory-grade systems, the placement of 24 FSRs per insole

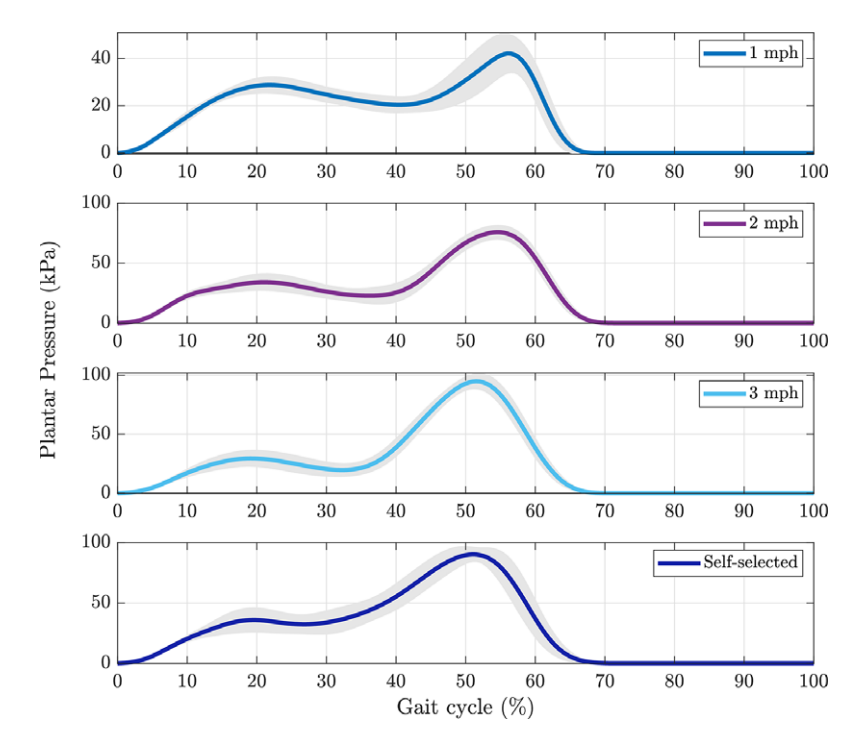


Figure 13. Plantar pressure obtained in the tests with a healthy female participant.

| Speed | | Peak force (kPa |) | | | Time (%) | | |
|-----------|-------|-----------------|-------|------|------|----------|------|------|
| | FA | FB | FC | TA | ТВ | TC | TD | TS |
| 1 mph | 28.78 | 20.40 | 42.13 | 22.0 | 40.5 | 56.0 | 68.0 | 32.0 |
| 2 mph | 34.12 | 22.74 | 75.72 | 21.5 | 36.0 | 54.5 | 70.5 | 29.5 |
| 3 mph | 29.51 | 19.60 | 94.80 | 19.5 | 32.0 | 51.5 | 69.5 | 30.5 |
| Free gait | 35.88 | 32.32 | 90.26 | 19.5 | 27.0 | 51.0 | 70.5 | 29.5 |

Table 5. Variables analyzed for plantar pressure during the gait cycle

across 10 anatomical regions offers a relatively dense layout that supports approximate pressure distribution analysis and functional gait pattern identification in portable applications.

- Accuracy compared to laboratory-grade systems: The developed system provides a cost-effective
 and portable alternative to conventional gait analysis tools. Nevertheless, its accuracy is lower
 than that of laboratory-grade systems such as pressure platforms and optical motion capture
 systems. Future work should include a formal comparison with reference systems to quantify these
 differences.
- Insole size: The instrumented insoles were developed in a single size (25.5 cm in length) for practical reasons and to focus on evaluating the system's technical integration. While this facilitated consistency in initial testing, it limits applicability to broader populations. The design is adaptable and could be scaled to different sizes in future iterations to support more extensive user studies and improve generalizability.
- Future improvements: To enhance usability and performance, future work will focus on testing a larger number of subjects for more rigorous statistical analysis. Additionally, routines involving actions such as going up and downstairs will be included, as well as a larger number of sensors. In addition, developing multisize versions of the insole and conducting large-scale validation studies are essential steps for broader deployment.

6. Conclusion

In this work, a portable system composed of two instrumented insoles, modules equipped with IMU and sEMG sensors, and software for indoor and outdoor environments was developed by implementing Wi-Fi connection and compact design of the structural elements of the measurement modules. The system demonstrated an average synchronization accuracy of $576\,\mu s$, ensuring proper time alignment between the signals of the different modules. In addition, a data loss of 0.8% was achieved, suggesting a reliable wireless transmission over the UDP protocol. Finally, the autonomy of 167 min of continuous operation allows its use in prolonged data acquisition sessions without interruptions, proving the functionality and versatility for the simultaneous acquisition of kinematic and kinetic signals from different devices. On the other hand, the evaluation of the collected signals allowed the analysis of relevant parameters in the study of gait, such as plantar pressure peaks; signal-to-noise ratio, change of slope sign, and waveform length for EMG evaluation; and angular ranges of the hip and knee joints, representing a qualitative and quantitative tool for gait analysis in various contexts, including applications in rehabilitation, biomechanics, and assistive technology development.

Data availability statement. The data that support the findings of this study are available on request from the corresponding author. The data are not publicly available due to privacy or ethical restrictions.

Acknowledgments. M. Alegria and M. Gomez-Correa acknowledge the scholarship from the SECIHTI, CVU: 1274683 and CVU: 1242726.

Author contribution. D.C. and M.B. were in charge of the conceptualization and supervised the project development. M.G. and M.A. conducted the experiments. M.G. developed the software. M.G. and M.A. developed the hardware of the system. Finally, all authors discussed the results and contributed to the final manuscript.

Funding statement. This research was supported by the Instituto Politécnico Nacional, grants SIP-20250223, SIP-20250253, SIP-20254832, and by the Secretaría de Educación, Ciencia, Tecnología e Innovación de la Ciudad de México (SECTEI) under the grant SECTEI/081/2024.

Competing interests. The authors declare no competing interests exist.

Ethical standard. The research meets all ethical guidelines, including adherence to the legal requirements of the study country.

References

Agostini V, Ghislieri M, Rosati S, Balestra G and Knaflitz M (2020) Surface electromyography applied to gait analysis: How to improve its impact in clinics? *Frontiers in Neurology* **994**, 1–13.

Alegria M, Alvarado C, Ballesteros M, Tobon-Vallejo D and Cruz-Ortiz D (2023) Development of a wearable device for analyzing plantar load in the human gait cycle. In 2023 11th International Conference on Control, Mechatronics and Automation (ICCMA). Adger, Norway: IEEE, pp. 7–12.

Alegria M, Ballesteros M and Cruz-Ortiz D (2025) A wireless instrumented insole for monitoring plantar pressure during human locomotion. Sensing and Bio-Sensing Research 47, 100752.

Anwary AR, Yu H and Vassallo M (2018) Optimal foot location for placing wearable IMU sensors and automatic feature extraction for gait analysis. *IEEE Sensors Journal* **18**(6), 2555–2567.

Arteaga MV, Castiblanco JC, Mondragon IF, Colorado JD and Alvarado-Rojas C (2020) EMG-driven hand model based on the classification of individual finger movements. *Biomedical Signal Processing and Control* 58, 101834.

Bagwell JJ, Avila E, Reynolds N, Smith JA, Valenzuela K and Katsavelis D (2024) Running Biomechanics Differ during and after Pregnancy Compared to Females Who Have Never Been Pregnant. Netherlands: Gait & Posture.

Benson LC, Clermont CA, Bošnjak E and Ferber R (2018) The use of wearable devices for walking and running gait analysis outside of the lab: A systematic review. *Gait & Posture* **63**, 124–138.

Benson LC, Räisänen AM, Clermont CA and Ferber R (2022) Is this the real life, or is this just laboratory? A scoping review of IMU-based running gait analysis. *Sensors* 22(5), 1722.

Bovi G, Rabuffetti M, Mazzoleni P and Ferrarin M (2011) A multiple-task gait analysis approach: Kinematic, kinetic and EMG reference data for healthy young and adult subjects. *Gait & Posture* 33(1), 6–13.

Burtscher J, Moraud EM, Malatesta D, Millet GP, Bally JF and Patoz A (2024) Exercise and gait/movement analyses in treatment and diagnosis of Parkinson's disease. *Ageing Research Reviews* 93, 102147.

Caramia C, Torricelli D, Schmid M, Munoz-Gonzalez A, Gonzalez-Vargas J, Grandas F and Pons JL (2018) IMU-based classification of Parkinson's disease from gait: A sensitivity analysis on sensor location and feature selection. *IEEE Journal of Biomedical and Health Informatics* 22(6), 1765–1774.

- Chen S, Lach J, Lo B and Yang GZ (2016) Toward pervasive gait analysis with wearable sensors: A systematic review. *IEEE Journal of Biomedical and Health Informatics* 20(6), 1521–1537.
- Choi W, Yang W, Na J, Lee G and Nam W (2021) Feature optimization for gait phase estimation with a genetic algorithm and Bayesian optimization. *Applied Sciences* 11(19), 8940.
- Cimorelli A, Patel A, Karakostas T and Cotton RJ (2024) Validation of portable in-clinic video-based gait analysis for prosthesis users. Scientific Reports 14(1), 3840.
- Ciniglio A, Guiotto A, Spolaor F and Sawacha Z (2021) The design and simulation of a 16-sensors plantar pressure insole layout for different applications: From sports to clinics, a pilot study. Sensors 21(4), 1450.
- Daunoraviciene K, Ziziene J, Pauk J, Juskeniene G and Raistenskis J (2021) EMG based analysis of gait symmetry in healthy children. Sensors 21(17), 5983.
- Delsys (n.d.) TRIGNO. Available at https://delsys.com/trigno.
- Felius R, Geerars M, Bruijn S, Wouda N, Van Dieën J and Punt M (2022) Reliability of IMU-based balance assessment in clinical stroke rehabilitation. *Gait & Posture* 98, 62–68.
- Fiker R, Kim LH, Molina LA, Chomiak T and Whelan PJ (2020) Visual gait lab: A user-friendly approach to gait analysis. Journal of Neuroscience Methods 341, 108775.
- Giacomozzi C, Keijsers N, Pataky T and Rosenbaum D (2012) International scientific consensus on medical plantar pressure measurement devices: Technical requirements and performance. Annali dell'Istituto superiore di sanita 48, 259–271.
- Haque F, Reaz MBI, Chowdhury MEH, Ezeddin M, Kiranyaz S, Alhatou M, Ali SHM, Bakar AAA and Srivastava G (2022) Machine learning-based diabetic neuropathy and previous foot ulceration patients detection using electromyography and ground reaction forces during gait. Sensors 22(9), 3507.
- Hermens HJ, Freriks B, Disselhorst-Klug C and Rau G (2000) Development of recommendations for SEMG sensors and sensor placement procedures. *Journal of Electromyography and Kinesiology* **10**(5), 361–374.
- Hussain I and Park SJ (2021) Prediction of myoelectric biomarkers in post-stroke gait. Sensors 21(16), 5334.
- Ichinohe T, Takahashi H and Fujita Y (2022) Force plate analysis of ground reaction forces in relation to gait velocity of healthy beagles. *American Journal of Veterinary Research* 83(9), 9–30.
- **Madgwick**, S. O., Harrison, A. J., & Vaidyanathan, R. (2011). Estimation of IMU and MARG orientation using a gradient descent algorithm. In 2011 IEEE international conference on rehabilitation robotics. IEEE, pp. 1–7.
- Mason R, Pearson LT, Barry G, Young F, Lennon O, Godfrey A and Stuart S (2023) Wearables for running gait analysis: A systematic review. *Sports Medicine* **53**(1), 241–268.
- Mobbs RJ, Perring J, Raj SM, Maharaj M, Yoong NKM, Sy LW, Fonseka RD, Natarajan P and Choy WJ (2022) Gait metrics analysis utilizing single-point inertial measurement units: A systematic review. *Mhealth* 83(9), 1–7.
- Monoli C, Fuentez-Pérez JF, Cau N, Capodaglio P, Galli M and Tuhtan JA (2021) Land and underwater gait analysis using wearable IMU. *IEEE Sensors Journal* 21(9), 11192–11202.
- Moreira L, Figueiredo J, Fonseca P, Vilas-Boas JP and Santos CP (2021) Lower limb kinematic, kinetic, and EMG data from young healthy humans during walking at controlled speeds. *Scientific Data* 8(1), 103.
- Negi S, CBS Negi P, Sharma S and Sharma N (2020) Electromyographic and acceleration signals-based gait phase analysis for multiple terrain classification using deep learning. *International Journal of Advanced Research in Engineering and Technology* 11(6), 656–665.
- Negi S, Sharma S and Sharma N (2021) FSR and IMU sensors-based human gait phase detection and its correlation with EMG signal for different terrain walk. Sensor Review 41(3), 235–245.
- Noraxon (n.d.) NORAXON. Available at https://www.noraxon.com/.
- Pancholi S and Joshi AM (2018) Portable EMG data acquisition module for upper limb prosthesis application. *IEEE Sensors Journal* 18(8), 3436–3443.
- Panebianco GP, Bisi MC, Stagni R and Fantozzi S (2018) Analysis of the performance of 17 algorithms from a systematic review: Influence of sensor position, analysed variable and computational approach in gait timing estimation from IMU measurements. Gait & Posture 66, 76–82.
- Park S and Yoon S (2021) Validity evaluation of an inertial measurement unit (IMU) in gait analysis using statistical parametric mapping (SPM). Sensors 21(11), 3667.
- Rahman MM, Gan KB, Aziz NAA, Huong A and You HW (2023) Upper limb joint angle estimation using wearable IMUs and personalized calibration algorithm. *Mathematics* 11(4), 970.
- Ribeiro NF and Santos CP (2017) Inertial measurement units: A brief state of the art on gait analysis. In *Placeholder Text2017 IEEE 5th Portuguese Meeting on Bioengineering (ENBENG)*. Coimbra, Portugal: IEEE, pp. 1–4.
- Rossi F, Mongardi A, Ros PM, Roch MR, Martina M and Demarchi D (2021) Tutorial: A versatile bio-inspired system for processing and transmission of muscular information. *IEEE Sensors Journal* 21(20), 22285–22303.
- Salis F, Bertuletti S, Bonci T, Caruso M, Scott K, Alcock L, Buckley E, Gazit E, Hansen C, Schwickert L, Aminian K, Becker C, Brown P, Carsin A-E, Caulfield B, Chiari L, D'Ascanio I, Del Din S, Eskofier BM, Garcia-Aymerich J, Hausdorff JM, Hume EC, Kirk C, Kluge F, Koch S, Kuederle A, Maetzler W, Micó-Amigo EM, Mueller A, Neatrour I, Paraschiv-Ionescu A, Palmerini L, Yarnall AJ, Rochester L, Sharrack B, Singleton D, Vereijken B, Vogiatzis I, Della Croce U, Mazzà C, Cereatti A and For The Mobilise-D Consortiu (2023) A multi-sensor wearable system for the assessment of diseased gait in real-world conditions. Frontiers in Bioengineering and Biotechnology 11, 1143248.

Sarshar M, Polturi S and Schega L (2021) Gait phase estimation by using LSTM in IMU-based gait analysis—Proof of concept. Sensors 21(17), 5749.

Seo K, Park YJ, Lee J, Hyung S, Lee M, Kim J, Choi H and Shim Y (2019) RNN-based on-line continuous gait phase estimation from shank-mounted IMUs to control ankle exoskeletons. In 2019 IEEE 16th International Conference on Rehabilitation Robotics (ICORR). Toronto, Ontario, Canada: IEEE, pp. 809–815.

Takeda R, Tadano S, Natorigawa A, Todoh M and Yoshinari S (2009) Gait posture estimation using wearable acceleration and gyro sensors. *Journal of Biomechanics* 42(15), 2486–2494.

Tao W, Liu T, Zheng R and Feng H (2012) Gait analysis using wearable sensors. Sensors 12(2), 2255–2283.

Tekscan (2018) Best practices in electrical integration of the FlexiForce sensor. Technical report. Tekscan. Available at https://www.tekscan.com/sites/default/files/FLX-Best-Practice-Electrical-Integration-RevB.pdf.

Tekscan (2024) Best practices in mechanical integration of the FlexiForceTM sensor. Technical report. Tekscan. Available at https://lp.tekscan.com/hubfs/FLX/FLX-Best-Practice-Mechanical-Integration-2.0.pdf?hsCtaAttrib=175807800197.

Trautmann J, Zhou L, Brahms CM, Tunca C, Ersoy C, Granacher U and Arnrich B (2021) Tripod—A treadmill walking dataset with imu, pressure-distribution and photoelectric data for gait analysis. Data 6(9), 95.

Tsakanikas V, Ntanis A, Rigas G, Androutsos C, Boucharas D, Tachos N, Skaramagkas V, Chatzaki C, Kefalopoulou Z, Tsiknakis M and Fotiadis D (2023) Evaluating gait impairment in Parkinson's disease from instrumented insole and IMU sensor data. *Sensors* 23(8), 3902.

Wang L, Jones D, Chapman GJ, Siddle HJ, Russell DA, Alazmani A and Culmer P (2019) A review of wearable sensor systems to monitor plantar loading in the assessment of diabetic foot ulcers. *IEEE Transactions on Biomedical Engineering* 67(7), 1989–2004.

Wang L, Sun Y, Li Q, Liu T and Yi J (2020) Two shank-mounted IMUs-based gait analysis and classification for neurological disease patients. IEEE Robotics and Automation Letters 5(2), 1970–1976.

Yamamoto M, Shimatani K, Ishige Y and Takemura H (2022) Verification of gait analysis method fusing camera-based pose estimation and an IMU sensor in various gait conditions. *Scientific Reports* 12(1), 17719.

Yu L, Mei Q, Xiang L, Liu W, Mohamad NI, István B, Fernandez J and Gu Y (2021) Principal component analysis of the running ground reaction forces with different speeds. Frontiers in Bioengineering and Biotechnology 9, 629809.

Ziagkas E, Loukovitis A, Zekakos DX, Chau TDP, Petrelis A and Grouios G (2021) A novel tool for gait analysis: Validation study of the smart insole podosmart®. Sensors 21(17), 5972.

Appendix A. Insoles characterization

The instrumented insoles were characterized following Tekscan's (2018) recommendations, where the first step consists of defining the maximum pressure the sensor must measure to adjust the sensitivity of each sensor, in this case, 24 N.

Then, similarly to Alegria et al. (2023), the calibration of each sensor was obtained by using a Mark-10 Series 5 digital dynamometer, considering four series of measures from 3 to 21 N with increments of 1 N (equivalent to 40.5 kPa). Therefore, a second-order fitting polynomial can describe the relationship between the pressure applied to each FSR and the output voltage. Then, introduce the following equation:

$$P_{ij} = a_{ij}C_{i,j}^3 + b_{ij}C_{i,j}^2 + c_{i,j}C_{i,j} + d_{i,j}$$
(A.1)

where $P_{i,j}$ is the pressure on the i,jth resistive sensor, see Figure 3, given in kPa, with $i = \{1,2,...,24\}$, $j = \{L,R\}$, $C_{i,j}$ denoting the value voltage registered by the ADC on a scale from 0 to 4,095. The constants $a_{i,j}$, $b_{i,j}$, $c_{i,j}$, and $d_{i,j}$ correspond to the coefficients of the fitting polynomial of each sensor, which are reported in Table A1.

 $a_{i,i}^{a}$ $b_{i,i}^{a}$ $c_{i,j}$ $d_{i,i}$ R R L Sensor L L L R R 4.1863 0.2652 -0.16290.0728 0.4249 -0.1190-169.0997.35 R_1 -0.08790.7849 0.0670 0.0302 -0.04170.0185 47.39 30.19 R_2 R_3 0.3515 5.5057 0.0270 -0.10000.0549 0.1664 10.74 -25.27 R_4 1.4259 2.7308 -0.0213-0.08560.12040.2559 -16.58-93.33 R_5 5.9501 -0.2902-0.19150.0992 0.4054 -0.1707-166.81132.58 R_6 22.4500 -0.96590.1305 1.5630 -685.00108.15 -1.1342-0.1618 R_7 1.8999 0.3414 -0.08810.0472 0.3642 -0.0144-201.5237.49 R_8 9.6200 0.1023 -0.37360.0506 0.6711 -0.0395-292.8347.66 R_9 3.8209 0.8792 -0.1753-0.01240.4645 0.1044 -214.93-10.560.0212 R_{10} 0.3087 4.6325 -0.16620.0698 0.7161 -1.28-352.26-0.97282.6045 0.0974 -0.07490.0711 -8.720.1665 -32.64 R_{11}

Table A1. Coefficients of the polynomial adjustment

(Continued)

Table A1 Continued

| | $a_{\mathrm{i,j}}{}^{\mathrm{a}}$ | | $b_{i,j}{}^{\mathrm{a}}$ | | $c_{i,j}$ | | $d_{ m i,j}$ | |
|----------|-----------------------------------|--------|--------------------------|---------|-----------|--------|--------------|---------|
| Sensor | L | R | L | R | L | R | L | R |
| R_{12} | 3.5235 | 4.9741 | -0.1131 | -0.1907 | 0.3585 | 0.3961 | -148.07 | -158.91 |
| R_{13} | 5.7699 | 3.8946 | -0.2374 | -0.1616 | 0.5087 | 0.3709 | -222.54 | -128.20 |
| R_{14} | 3.0605 | 1.8507 | -0.1481 | -0.0854 | 0.4170 | 0.2853 | -197.95 | -127.93 |
| R_{15} | 3.9487 | 1.7104 | -0.1496 | -0.0349 | 0.3154 | 0.1390 | -98.79 | -23.89 |
| R_{16} | 7.8883 | 7.1092 | -0.2815 | -0.3383 | 0.5371 | 0.7079 | -218.14 | -301.19 |
| R_{17} | 4.9560 | 1.1490 | -0.1531 | -0.0246 | 0.5539 | 0.1079 | -293.87 | -33.64 |
| R_{18} | 1.7304 | 8.7133 | -0.0563 | -0.4045 | 0.2461 | 0.7655 | -102.26 | -353.35 |
| R_{19} | 147.5129 | 2.3613 | -4.7609 | -0.1127 | 5.4841 | 0.4097 | -2017.65 | -200.82 |
| R_{20} | 5.5224 | 4.5323 | -0.2050 | -0.2213 | 0.4021 | 0.5636 | -151.83 | -230.33 |
| R_{21} | 44.7369 | 5.3217 | -1.5339 | -0.2184 | 2.0613 | 0.4507 | -792.89 | -181.54 |
| R_{22} | 2.4258 | 1.4444 | -0.0825 | -0.0411 | 0.2328 | 0.2181 | -58.96 | -96.94 |
| R_{23} | 0.7536 | 0.2150 | -0.0139 | 0.0189 | 0.1582 | 0.1081 | -37.99 | -2.16 |
| R_{24} | 5.8667 | 6.8969 | -0.2607 | -0.3076 | 0.5522 | 0.6314 | -233.83 | -262.09 |

^aThe coefficients $a_{i,j}$ are expressed on a scale of $\times 10^{-8}$, while coefficients $b_{i,j}$ are on a scale of $\times 10^{-3}$.